sensors

MDPI

Article

Surface Potential-Controlled Oscillation in FET-Based Biosensors

Ji Hyun Kim [1,†], Seong Jun Park [1,†], Jin-Woo Han [2] and Jae-Hyuk Ahn [3,*]

[1] Department of Electronic Engineering, Kwangwoon University, Seoul 01897, Korea; jayyullmoo@naver.com (J.H.K.); sjun96@naver.com (S.J.P.)
[2] Center for Nanotechnology, NASA Ames Research Center, Mountain View, CA 94035, USA; jin-woo.han@nasa.gov
[3] Department of Electronics Engineering, Chungnam National University, Daejeon 34134, Korea
* Correspondence: jaehyuk@cnu.ac.kr
† These authors contributed equally to this work.

Abstract: Field-effect transistor (FET)-based biosensors have garnered significant attention for their label-free electrical detection of charged biomolecules. Whereas conventional output parameters such as threshold voltage and channel current have been widely used for the detection and quantitation of analytes of interest, they require bulky instruments and specialized readout circuits, which often limit point-of-care testing applications. In this study, we demonstrate a simple conversion method that transforms the surface potential into an oscillating signal as an output of the FET-based biosensor. The oscillation frequency is proposed as a parameter for FET-based biosensors owing to its intrinsic advantages of simple and compact implementation of readout circuits as well as high compatibility with neuromorphic applications. An extended-gate biosensor comprising an Al_2O_3-deposited sensing electrode and a readout transistor is connected to a ring oscillator that generates surface potential-controlled oscillation for pH sensing. Electrical measurement of the oscillation frequency as a function of pH reveals that the oscillation frequency can be used as a sensitive and reliable output parameter in FET-based biosensors for the detection of chemical and biological species. We confirmed that the oscillation frequency is directly correlated with the threshold voltage. For signal amplification, the effects of circuit parameters on pH sensitivity are investigated using different methods, including electrical measurements, analytical calculations, and circuit simulations. An Arduino board to measure the oscillation frequency is integrated with the proposed sensor to enable portable and real-time pH measurement for point-of-care testing applications.

Keywords: field-effect transistor; chemical and biological sensor; pH sensor; surface potential; oscillation frequency; ring oscillator; extended gate

check for updates

Citation: Kim, J.H.; Park, S.J.; Han, J.-W.; Ahn, J.-H. Surface Potential-Controlled Oscillation in FET-Based Biosensors. *Sensors* **2021**, *21*, 1939. https://doi.org/10.3390/s21061939

Academic Editors: Pedro Estrela and Jae-Hyuk Ahn

Received: 10 February 2021
Accepted: 5 March 2021
Published: 10 March 2021

Publisher's Note: MDPI stays neutral with regard to jurisdictional claims in published maps and institutional affiliations.

Copyright: © 2021 by the authors. Licensee MDPI, Basel, Switzerland. This article is an open access article distributed under the terms and conditions of the Creative Commons Attribution (CC BY) license (https://creativecommons.org/licenses/by/4.0/).

1. Introduction

Field-effect transistor (FET)-based biosensors have received significant attention for their label-free electrical detection of chemical and biological species. Because of their inherent similarity with conventional FETs in terms of device structure and fabrication process, FET-based biosensors offer the well-known advantages of modern electronic devices such as high-density integration of sensor arrays in a compact size, reliable fabrication with high reproducibility, and low-cost mass fabrication. The replacement of the solid-state gate of a conventional FET to the liquid–solid interface allows an FET-based biosensor to have an open surface for detecting chemical reactions or biological binding of interest. Since the invention of ion-sensitive field-effect transistors that facilitate the detection of ions by P. Bergveld in 1970 [1], FET-based biosensors have been widely utilized for detecting antibody–antigen [2–4], DNA [5,6], and viruses [7–9] for disease diagnosis, basic research, and point-of-care testing (POCT). Advanced nanotechnology and the discovery of new materials have improved sensing performances such as sensitivity and limit of detection by the incorporation of silicon nanowires [10–12], carbon nanotubes [13,14],

graphene [15–17], two-dimensional transition metal dichalcogenide [18,19], and metal oxide nanostructures [20–22] into basic elements of FET-based biosensors.

An FET-based biosensor transduces a binding event occurring on the gate surface into a change in the electrical characteristics, such as the threshold voltage or channel current [23–25]. For example, the reversible binding of hydrogen ions on the active sites of a gate (i.e., ion-sensitive membrane) results in a change in the surface potential of the channel; this phenomenon can be utilized in developing pH sensors [26,27]. When a receptor functionalized on an FET surface captures its analyte, the intrinsic charge of the analyte changes the surface potential of the FET. This mechanism enables label-free electrical detection of antibody-antigen binding and DNA binding [5,10,11]. Binding-induced conformational changes (i.e., aptamers) result in changes in the local potential near the FET surface [28–30]. The existence and quantity of analytes in a test solution are correlated with the amount of change in the threshold voltage or channel current. Hence, the threshold voltage and channel current have been widely used as output parameters for FET-based biosensors.

Among several methods for monitoring the threshold voltage and channel current, a parameter analyzer, which is a specialized equipment for characterizing the electrical properties of FET devices, is widely used for extracting output parameters owing to its precision measurement with high resolution [31–33]. However, its bulky size and exorbitant cost limit POCT applications. As an alternative for POCT applications, readout circuits for monitoring output parameters have been constructed in the form of small-sized integrated circuits (ICs) by using modern electronics technology [34,35]. Despite the portability of ICs, their customized fabrication and high cost in design and development limit their generic use in readout circuits.

The sensing process outputs analog values of both voltage and current readings. Subsequently, these analog values are digitalized using a readout circuit. Traditionally, the analog output is input into an analog-to-digital converter (ADC) to interface with digital electronics. This is associated with the fact that the traditional computer architecture, i.e., the von Neumann architecture, has long evolved digitally to countermeasure noise immunity. Recently, the neuromorphic architecture has attracted significant attention in mimicking the neurobiological structure of the nerve system [36–40]. One of the neuromorphic architectures is the spiking-neural network [41,42], which mimics the natural neural network the most. When the traditional ADC is integrated with the neuromorphic architecture, the ADC levels must be converted into spiking rates, thereby resulting in circuit inefficiency, propagation delay, and power consumption. Therefore, an alternative method that is the most compatible with spiking neural networks must be identified.

In this study, we demonstrate a signal conversion scheme using frequency as a new output parameter of FET-based biosensors to complement the conventional output parameters. The simple connection of a ring oscillator to a readout transistor enables the conversion from a surface potential to an oscillation signal. The oscillation frequency can be regarded as the spiking rate of the neural network. Hence, the frequency and spiking rate can be used interchangeably. The spiking rate as an output can be input into the axillary spiking neural network. To demonstrate the spiking rate altered by biosensing, in this study, the oscillation frequency is measured using a portable, general-purpose microcontroller (i.e., Arduino) by counting the number of peaks in a given time. Electrical measurement of the linear correlation between the oscillation frequency and pH value confirms that the oscillation frequency is a suitable output parameter for FET-based biosensors. We discuss the change in the pH sensitivity of the oscillation frequency based on experiments, analytical calculations, and circuit simulations. Finally, we present the future prospects of using the oscillation frequency in portable sensing systems based on real-time pH measurements using an Arduino board operated via open source codes.

2. Experimental Section

2.1. Fabrication of Sensing Electrodes

The fabrication of pH-sensitive electrodes was based on our previous study [9,43]. Briefly, a 15-nm-thick Al_2O_3 layer was deposited on metal electrodes (Cr/Au = 3 nm/100 nm) via electron beam evaporation. The dimensions of the metal electrodes were 3 mm × 3 mm or 5 mm × 5 mm. A reservoir to fill the test solution was constructed on the Al_2O_3 sensing layer using a silicone elastomer (Kwik-cast, World Precision Instruments, Inc., Sarasota, FL, USA). Optical microscopy images of the fabricated sensing electrodes are presented in Supplementary Materials (Figure S1).

2.2. Construction of Frequency Measurement System

A schematic illustration of the experimental setup is shown in Figure 1. A pH buffer solution was added to the reservoir constructed on the sensing electrode, and an Ag/AgCl reference electrode (MF-2052, Bioanalytical Systems, Inc., West Lafayette, IN, USA) was immersed in the test solution. The probing pad of the fabricated sensing electrode was connected to the gate terminal of a commercially available n-type FET (CD4007UBE, Texas Instruments, Dallas, TX, USA), which was used as a readout transistor to convert the surface potential of the sensing electrode to the drain current (I_D). This configuration is known as the extended-gate FET [44]. The control voltage (V_{ctrl}) terminal of a three-stage ring oscillator (CD4007UBE, Texas Instruments, Dallas, TX, USA) was connected to the drain terminal of the readout transistor, where the load resistor was connected. Two separate CD4007UBE devices were used to construct the readout transistor and three-stage ring oscillator. The ring oscillator arrangement using CD4007UBE devices is provided in Supplementary Materials (Figure S7b).

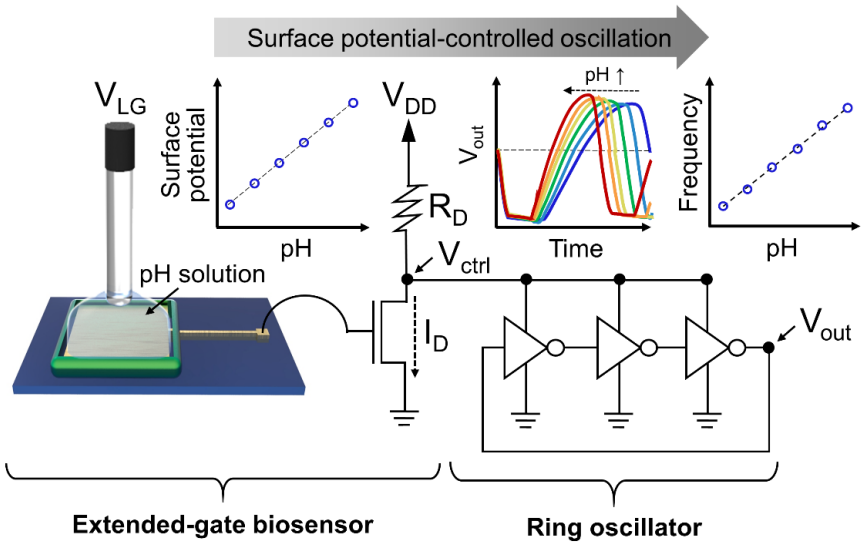

Figure 1. Schematic illustration of surface potential-controlled oscillation. An extended gate (i.e., sensing electrode) that generates surface potential based on pH is connected to a readout transistor, where surface potential is converted to drain current (I_D). Subsequently, I_D that flows through the load resistor (R_D) determines the control voltage (V_{ctrl}), which is input to the ring oscillator that generates an oscillation signal. Oscillation frequency is utilized as an output parameter for pH sensing.

2.3. Electrical Characterization

A liquid-gate voltage (V_{LG}) was applied to the reference electrode, and a supply voltage (V_{DD}) was applied to the load resistor connected to the drain terminal of the readout transistor using with a SourceMeter (Model 2614B, Keithley Instruments, Inc., Cleveland, OH, USA). The voltage drop in the load resistor determined the V_{ctrl} input to the

ring oscillator. The oscillation frequency of the ring oscillator was measured at the output terminal of the ring oscillator using an oscilloscope (EDUX1002A, Keysight Technologies, Santa Rosa, CA, USA). The threshold voltage (V_T), which is defined as the gate voltage that flows a I_D of 100 nA in the subthreshold region, was extracted using the SourceMeter by sweeping the V_{LG} and measuring the I_D after removing the load resistor and ring oscillator.

2.4. Portable Sensing System

An Arduino board (Arduino Uno R3, Arduino LLC, Somerville, MA, USA), which is a general-purpose microcontroller, was used to construct a portable sensing system to measure the oscillation frequency. A liquid crystal display (LCD) module (SZH-EK101, SMG, China) was connected to an Arduino board to display the measured frequency. All components including the sensing electrode, readout transistor, three-stage ring oscillator, Arduino board, and LCD module were integrated on a printed circuit board (PCB). A 9 V battery was used to supply power to each component. The detailed Arduino board-pin mapping and the applied voltages are shown in Figure S7. The Arduino source codes that counted the number of oscillations were uploaded to the Arduino board where the LCD was connected to display the oscillation frequency according to the pH. The Arduino source codes for the frequency measurement are provided in Supplementary Materials.

3. Results and Discussion

3.1. Operation Principle: Surface Potential-Controlled Oscillation

Compared with conventional FET-based biosensors, a distinctive feature of the proposed biosensor is the parameter conversion scheme constructed using a ring oscillator that converts the V_T or I_D to the oscillation frequency (Figure 1). Although we used a three-stage ring oscillator, it was not necessarily the best option. The number of stages allows the system designer to select the spiking rate of interest. Alternatively, increasing the supply voltage at a specified oscillator can be a method to increase the nominal point of the spiking rate. As the odd number of stages increases, the oscillation frequency can be decreased. The typical frequency range can vary from low frequency (~20 Hz), audio frequency (20 Hz–20 kHz), and up to radio frequency (100 kHz–100 GHz). Furthermore, other types of oscillators such as the resistor-capacitor or inductor-capacitor, or variations of the ring oscillator can be used as requred. The oscillation frequency can be measured using not only a bulky oscilloscope, but also using a compact, portable general-purpose microprocessor (i.e., Arduino board); this will be discussed later.

The operating mechanisms of extended-gate biosensors have been investigated previously [24]. A change in the surface potential of the sensing electrode upon the binding of chemical and biological species results in a change in the threshold voltage, consequently modulating the I_D of the readout transistor. The new components, i.e., the ring oscillator and load resistor, incorporated in the output of the extended-gate biosensor convert the I_D to the oscillation frequency. The amount of I_D flowing through the load resistor determines the voltage at the drain terminal (i.e., V_{ctrl}), which is the supply voltage of the subsequent ring oscillator where the oscillation frequency is changed by the value of V_{ctrl}. In the entire procedure, the surface potential of the sensing electrode results in an oscillation frequency, indicating that the frequency can be utilized as a new output parameter for FET-based biosensors.

3.2. pH Sensing Characteristics

We investigated the relationship between the oscillation frequency of the proposed sensor and the pH value of the test solution to verify the feasibility of the oscillation frequency as an output parameter for FET-based biosensors. The pH sensing experiment is a popular proof-of-concept example that confirms the ability of the newly designed sensor in detecting charged biomolecules [9,10,43]. With an increase in the pH value of the buffer solution, the output signal, which is the output voltage as a function of time, shifted to the

left, thereby increasing the oscillation frequency (Figure 2a,b). The frequency depended linearly on the pH value, with high reproducibility (Figure 2b,c).

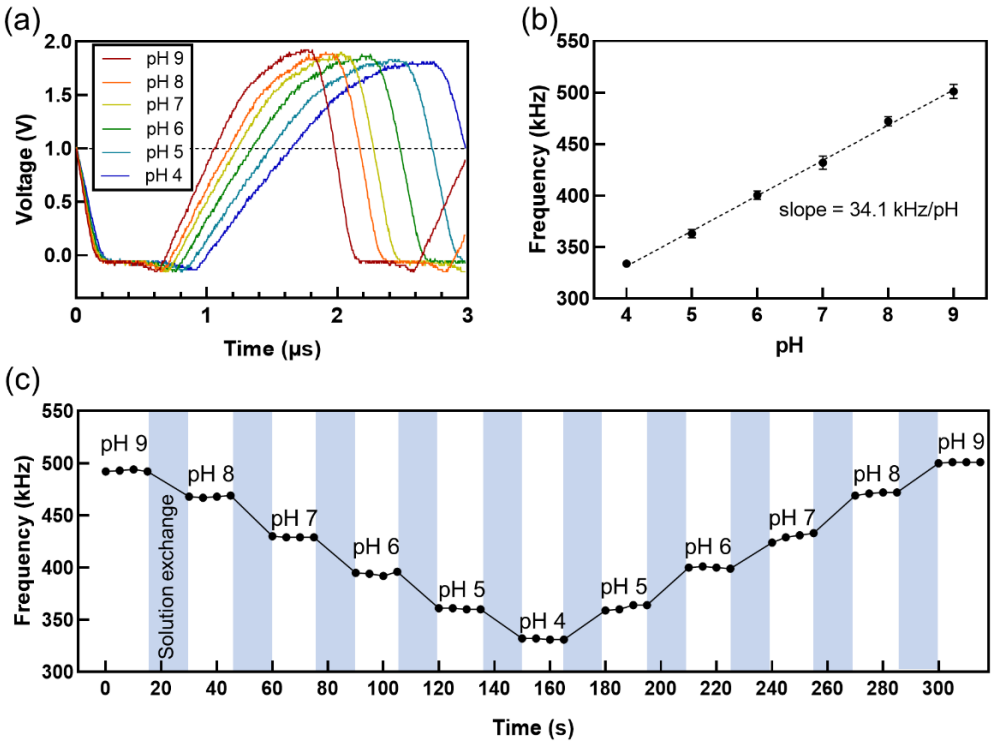

Figure 2. pH sensing characteristics. (**a**) Output waveform of ring oscillator as a function of pH. Starting point of each curve overlapped at 0 s. Dotted line provides visual guidance of shift in period (inverse of frequency) due to pH. (**b**) Oscillation frequency vs. pH, showing linear slope of 34.1 kHz/pH. (**c**) Time-resolved pH measurement. pH sensing results confirmed ability of proposed sensor in detecting changes in surface potential.

Our additional experiments revealed that the oscillation frequency was directly correlated with V_T. The same sensing electrode used to obtain Figure 2a,b shows a similar trend in terms of the linear dependence of V_T on pH (Figure S2). The pH-induced V_T shift can be explained by site-binding theory, in which hydrogen ions reversibly bind to active OH sites on the Al_2O_3 surface, thereby generating a surface potential based on pH [26,45]. When a sensing electrode indicates a nonlinear dependence of V_T on pH due to undesired defects on the surface, the oscillation frequency as a function of pH exhibits the same nonlinear trend, which does not facilitate correct measurements (Figure S3). This result implies that the preparation of sensing electrodes that generate sensitive and reliable surface potentials is crucial in the design of high-performance surface potential-controlled oscillations.

Further measurements indicate that V_T modulated the oscillation frequency. The oscillation frequency of the ring oscillator was proportional to the gate voltage (V_G) of the readout transistor via the transfer of V_G into V_{ctrl} (Figure S4). It is noteworthy that changing V_G in these measurements can be considered as a pH-induced V_T shift because V_T is defined as the effective V_G that flows a constant I_D. The close relationship between V_T and oscillation frequency allows the frequency to be a versatile output parameter without sacrificing the advantages of V_T in FET-based biosensors.

Although we simply measured a small pH range of 4 to 9 to demonstrate surface potential-controlled oscillation, the Al_2O_3-deposited sensing electrode can detect a wider pH range of 3 to 11, as confirmed by the pH sensing characteristics of our previous study [46]. The maximum V_T shift (i.e., voltage signal) is measured as ~0.4 V from pH 3 to 11. A curve for the oscillation frequency as a function of the gate voltage (Figure S4d) shows that an input signal larger than 0.5 V can be linearly converted to the oscillation

frequency. Because the allowed input voltage for linear frequency conversion is larger than the maximum voltage signal generated from the sensing electrode, our sensor is expected to measure the pH response of the Al_2O_3 surface over a pH range of 3 to 11.

It is expected that the pH sensitivity depends on the temperature because the surface potential (ψ_o) of the sensing electrode can be described with the Nernst equation [26]:

$$\psi_o = 2.303\frac{kT}{q}\log[a_{H^+}/a_{H^+}{}^o]$$

where k is the Boltzmann constant, T is the absolute temperature, q is the elementary charge, a_{H^+} is the solution's ion activity, and $a_{H^+}{}^o$ is the ion activity at the point of zero charge. In our previous study, the Al_2O_3-deposited electrode generated 43.7 mV/pH at 25 °C (298 K) and 45.4 mV/pH at 40 °C (313 K), where the pH sensitivity improvement by 4% is similar to the Nernst equation-derived calculation by 5% [46]. A similar temperature dependence on pH sensitivity has been reported elsewhere [27]. This temperature instability should be further compensated in a readout circuit by measuring the test solution temperature.

It is possible to detect biomolecular interactions in real time if the sensing electrode is functionalized with receptors to capture target biomolecules. However, nonspecific binding of interfering biomolecules present in serum and blood generates noises to deteriorate detection sensitivity. To prevent nonspecific binding on the sensing electrode, the remaining binding sites on the surface are generally blocked by a bovine serum albumin (BSA) solution [32,47]. In addition, tailoring the sensor surface with a polymer polyethylene glycol (PEG) can further reduce nonspecific signals from interfering biomolecules owing to the hydrophilic PEG on the surface, which enables real-time immunodetection in whole serum [47,48].

3.3. Signal Amplification

Understanding the effects of circuit parameters on the frequency signal is important when establishihng methods for signal amplification. Unlike the V_T signal, which requires dual gates for siginal amplificaiton [12,25,49,50], the single-gate configuration is sufficient for increasing the frequency sensitivity in units of Hz/pH by controlling the values of other circuit parameters, such as the number of stages (N), load resistance (R_D), and V_{LG}.

Figure 3a shows the frequency as a function of pH for N = 3, 5, and 7. The sensitivity increased as N decreased (Figure 3b). The frequency of the ring oscillator (f) can be modeled as $f = 1/(2Nt_p)$, where t_p is the propagation delay time per stage. Let us assume that the per-stage delay change from the initial value is $\Delta t_p = t_p - t_{p,i}$ at a given pH. Therefore, the frequency change, i.e., the sensitivity, $\Delta f = -\Delta t_p / (2Nt_p t_{p,i})$. Because t_p and $t_{p,i}$ are independent of N, the simple frequency change model reveals that a lower N results in a higher sensitivity. Despite its lower sensitivity at N = 7, its lower operating frequency implies that high-performance circuits are not necessitated for measuring high frequencies, hence the tradeoff between sensitivity and operating frequency in terms of N.

Similar pH sensing experiments were performed to investigate the effect of R_D on sensitivity (Figure 3c). Figure 3d shows that the sensitivity increased with R_D. The oscillation frequency is a function of power effectively delivered by V_{ctrl}, where V_{ctrl} is obtained using the voltage divider circuit of the resistances of the load resistor and readout transistor. The voltage divider model of V_{ctrl} can be expressed as $V_{ctrl} / V_{DD} = R_T / (R_D + R_T)$, where R_T is a function of I_D or V_T of the readout transistor. Consequently, a higher R_D results in a lower operation frequency. The effect of the load resistor on the sensitivity can be directly explained based on V_{ctrl}. In other words, the gain of the readout is translated into the pH sensitivity. The small voltage variation due to the pH value multiplied by the transconductance g_m of the readout transistor is the I_D variation. According to Ohm's law ($V = IR$), for the voltage divider of the load resistor and readout transistor, the I_D variation multiplied by the load resistance yields V_{ctrl} variation. Consequently, the gain of the readout circuit or sensitivity is $g_m \cdot R_D$. A higher transconductance and a higher R_D result in a more sensitive sensor. However, when R_D is excessively large, the voltage drop

across the load resistor can be dominant, and V_{ctrl} becomes extremely low. In this case, the swing of V_{ctrl} and the sensor resolution can be limited. In extreme cases, V_{ctrl} can vary nonlinearly with pH because of the small swing.

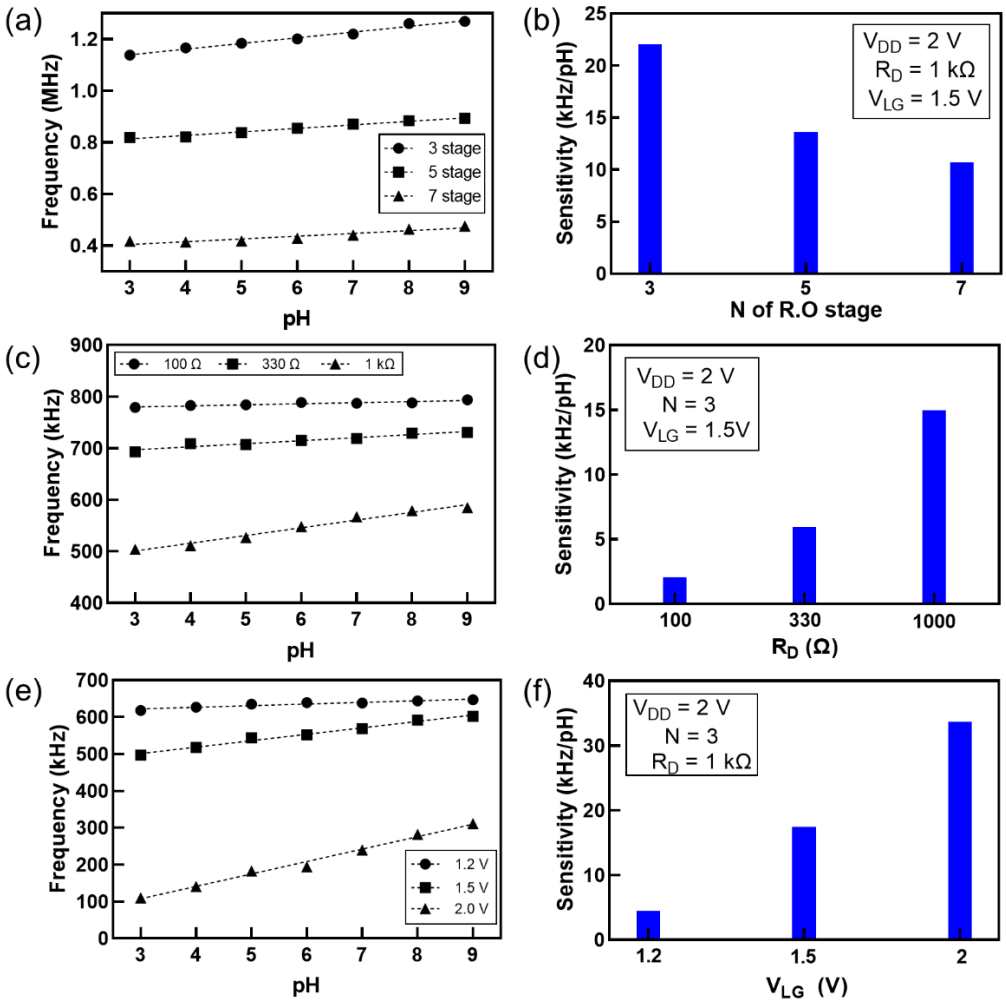

Figure 3. Effects of circuit parameters on sensitivity. (**a**) Oscillation frequency vs. pH for different numbers of stages (N). (**b**) Dependence of sensitivity on N. (**c**) Oscillation frequency vs. pH for different values of load resistance (R_D). (**d**) Dependence of sensitivity on R_D. (**e**) Oscillation frequency vs. pH for different values of liquid-gate voltage (V_{LG}). (**f**) Dependence of sensitivity on V_{LG}.

Finally, the effect of V_{LG} on sensitivity was analyzed, as shown in Figure 3e. Figure 3f shows that the sensitivity increases with the V_{LG}. As explained earlier, the gain of the readout transistor or the sensitivity of the sensor is $g_m \cdot R_D$, where g_m increases with the DC gate bias of the readout transistor. However, if the DC gate bias increases significant, more I_D will flow and the gain will be compromised by power consumption. This is particularly important if the sensor is intended for an always-on application. In addition, similar to the voltage swing of V_{ctrl} being constrained by a high R_D, a high g_m yields the same result. Therefore, the tradeoff between sensitivity and nonlinearity/resolution/power consumption must be considered.

These experiments were consistent with an analytical equation that indicates the same dependence of the circuit parameters (N, R_D, and V_{LG}) on the frequency sensitivity (See Section 3.4):

$$\frac{df}{dpH} \propto \frac{(V_{LG} - V_{\mathrm{T}})R_D}{N},$$

where V_T is the threshold voltage of the readout transistor. Furthermore, the circuit simulations exhibited the same effects of the circuit parameters (N, R_D, and V_{LG}) on the frequency sensitivity (Figure S5). Understanding of signal amplification will be beneficial to the future design of highly sensitive frequency-based biosensors.

3.4. Analytical Equation for Investigating Effects of Circuit Parameters on Sensitivity

To increase the sensitivity of the sensor, we derived a theoretical equation to express the effect of each circuit parameter on the sensitivity. The sensitivity can be calculated by taking the derivative of the oscillation frequency (f) with respect to the pH, as follows:

$$\frac{df}{dpH} = \frac{dV_T}{dpH}\frac{dV_{ctrl}}{dV_T}\frac{df}{dV_{ctrl}} = \alpha\frac{dV_{ctrl}}{dV_T}\frac{df}{dV_{ctrl}} \tag{1}$$

where $\alpha = dV_T / dpH$ is the pH sensitivity of the Al_2O_3 sensing layer caused by a pH-based surface potential change.

The drain current I_D of the readout transistor biased in saturation is expressed as

$$I_D = \frac{1}{2}\mu_n C_{ox}\frac{W}{L}(V_{LG} - V_{\mathrm{T}})^2 = \frac{k}{2}(V_{LG} - V_{\mathrm{T}})^2 \tag{2}$$

where μ_n is the mobility of the electrons in the inversion layer, C_{ox} the oxide capacitance, W the channel length, and L the channel width, and parameter $k = \mu_n C_{ox} W / L$ includes geometry and technology-dependent parameters.

When the drain current I_D that flows through the load resistor R_D causes a voltage drop across the resistor, the control voltage V_{ctrl} can be expressed as

$$V_{ctrl} = V_{DD} - I_D R_D = V_{DD} - \frac{k}{2}(V_{LG} - V_{\mathrm{T}})^2 R_D \tag{3}$$

Subsequently, the second term in Equation (1) can be calculated by taking the derivative with respect to V_T as follows:

$$\frac{dV_{ctrl}}{dV_T} = k(V_{LG} - V_{\mathrm{T}})R_D \tag{4}$$

The oscillation frequency f is expressed as

$$f = \frac{1}{2Nt_p} \tag{5}$$

where N is the number of stages, and t_p is the propagation delay per stage. The delay time t_p is a function of the load capacitance (C_L), supply voltage of the ring oscillator (V_{ctrl}), and drain current (I_{Dsat}) that flows through the ring oscillator, as follows [51]:

$$t_p = \frac{C_L V_{ctrl}}{2I_{Dsat}} = \frac{C_L V_{ctrl}}{k(V_{ctrl} - V_{\mathrm{T0}})^2} \tag{6}$$

where V_{T0} is the ring oscillator threshold voltage. It is noteworthy that the ring oscillator has the same initial threshold voltage as the readout transistor because the same n-type transistors (CD4007UBE, Texas Instruments, Dallas, TX, USA) are used. However, in contrast to V_T, V_{T0} is not a function of pH.

Substituting Equation (6) into Equation (5) yields

$$f = \frac{1}{2N}\frac{k(V_{ctrl} - V_{\mathrm{T0}})^2}{C_L V_{ctrl}} \tag{7}$$

Subsequently, the third term in Equation (1) can be calculated by taking the derivative with respect to V_{ctrl}:

$$\frac{df}{dV_{ctrl}} = \frac{k}{2NC_L}\left(1 - \frac{{V_{T0}}^2}{{V_{ctrl}}^2}\right) \simeq \frac{k}{2NC_L} \tag{8}$$

Finally, the sensitivity equation is obtained using Equations (1), (4), and (8) as follows:

$$\frac{df}{dpH} = \alpha\frac{k^2}{2NC_L}(V_{LG} - V_T)R_D \tag{9}$$

The sensitivity increases as the number of stages N decreases, the load resistance R_D increases, and the liquid-gate voltage V_{LG} increases.

3.5. pH Sensing Using Portable System

A portable pH sensing system was constructed by replacing the bulky oscilloscope for the frequency measurement with a compact Arduino board, a general-purpose microprocessor capable of counting the number of oscillations via open-source codes (Figure 4a,b). Figure 4b shows that all the components for pH sensing, except the reference electrode, were integrated on a PCB board, on which the LCD screen was mounted to display the frequency measured according to the pH value of the test solution. The oscillation frequency in the portable sensing system increased with the pH value (Figure 4c), showing the same trend as that of the oscilloscope. The portable sensing system successfully demonstrated the real-time measurement of the pH response with high reproducibility (Figure 4d).

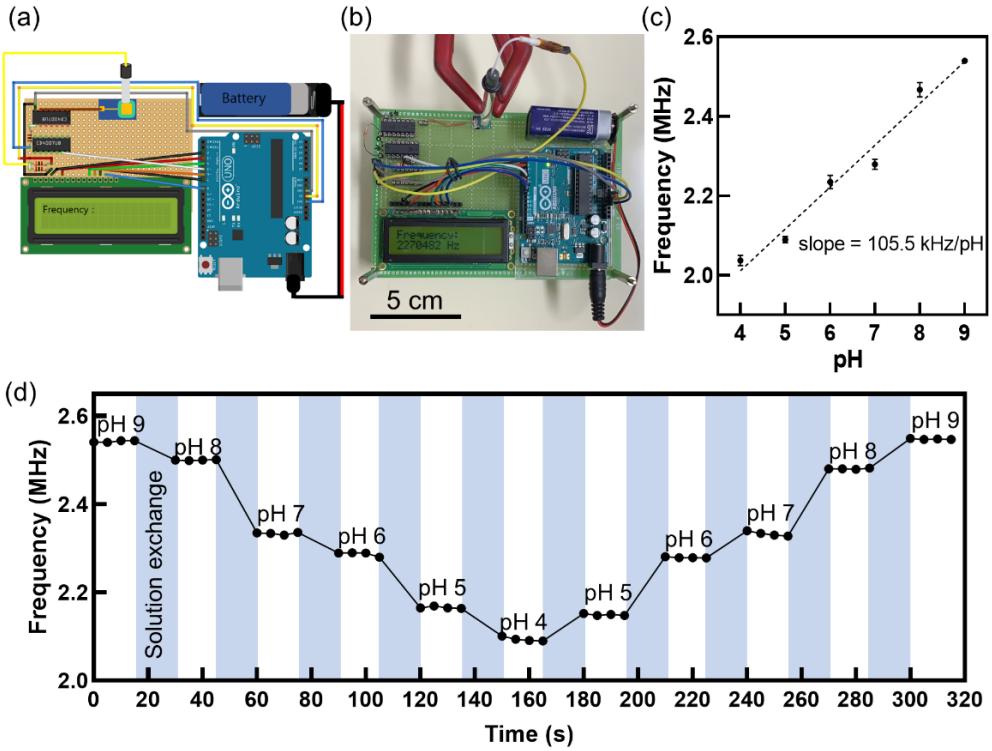

Figure 4. Portable measurement system. (**a**) Schematic illustration of portable measurement system. Small-sized Arduino board to replace bulk-sized oscilloscope for measuring oscillation frequency of sensor; 9 V battery supplies power to circuit. Operating conditions were V_{DD} = 3.3 V, V_{LG} = 2 V, R_D = 1 kΩ, and N = 3. (**b**) Optical image of portable measurement system. Measured frequency displayed on the LCD screen. (**c**) Oscillation frequency vs. pH. (**d**) Real-time measurement of pH using portable measurement system.

However, the portable sensing system requires futher developments for practical applications. First, the bulky Ag/AgCl reference electrode should be miniaturized to a

compact size. Recent studies have demonstrated such miniaturization using an integrated on-chip gold gate [52] or an integrated fluidic chamber comprising an agarose gel sealed with a UV-curable resign [53], which is compatible with our sensor fabrication. Second, the accuracy of the frequency measurement of the portable sensing system should be further improved such at it can detect target analytes in a small dynamic range of interest [54]. Because the output waveform of the ring oscillator is not an ideal sinusoidal waveform (Figure 2a), some errors may be generated during frequency extraction; however, they will be rectified via noise reduction using a Schmitt trigger (Figure S6).

Wireless signal transmission can be simply and inexpensively implemented by connecting a Bluetooth module to the Arduino and using a smartphone application [55,56]. Through the Bluetooth connection between the Arduino and the smartphone, sensing data from the Arduino can be transferred to the smartphone screen instead of the LCD, which will be a subject of our further work (Figure S8). This platform not only receives sensing data in real time, but is also promising and versatile for POCT applications.

4. Conclusions

We demonstrated a conversion method that enables surface potential-controlled oscillations to provide the oscillation frequency as an output parameter for FET-based biosensors. Unlike conventional parameters such as V_T and I_D, the oscillation frequency requires neither bulky and expensive analysis equipment nor complicated and specified ICs. However, it is compatible with open-source electronics platforms such as the Arduino board. The ring oscillator connected to the extended-gate biosensor can convert the pH-induced surface potential generated in the Al_2O_3 layer of the extended gate into an oscillation signal. The proposed sensor demonstrated sensitive and reliable pH sensing based on the linear dependence of the oscillation frequency on pH, suggesting the usefulness of the oscillation frequency for the analysis of FET-based biosensors. Our comparison of the V_T signal and oscillation frequency revealed that they were directly correlated with each other as well as with the surface potential, and that the sensing electrode that can produce a higher surface potential was key for signal amplification. The pH sensing experiments, analytical calculations, and circuit simulations confirmed that the frequency signal upon the pH response can be further amplified by controlling the circuit parameters, such as by reducing N, increasing R_D, and increasing V_{LG}. A portable sensing system for real-time pH measurement was constructed on a PCB board by integrating an extended-gate biosensor and an Arduino board to measure the frequency signal. The surface potential-controlled oscillation in this study is suitable for not only POCT applications, but also neuromorphic applications based on spiking neural networks.

Supplementary Materials: The following are available online at https://www.mdpi.com/1424-8220/21/6/1939/s1, Figure S1: Optical microscopy images of sensing electrode, Figure S2: pH sensing characteristics of extended-gate FET with Al_2O_3 layer, Figure S3: Comparison between threshold voltage and oscillation frequency, Figure S4: Conversion of gate voltage to oscillation frequency, Figure S5: PSpice simulations for investigating effects of circuit parameters on sensitivity, Figure S6: Comparison between performances of oscilloscope and Arduino, Figure S7: Arduino board-pin mapping, Arduino source codes for frequency measurement, and Figure S8: Wireless signal transmission.

Author Contributions: Conceptualization, J.-W.H. and J.-H.A.; formal analysis, J.H.K. and S.J.P.; investigation, J.H.K. and S.J.P.; writing—original draft preparation, J.H.K. and S.J.P.; writing—review and editing, J.-W.H. and J.-H.A.; supervision, J.-H.A.; funding acquisition, J.-H.A. All authors have read and agreed to the published version of the manuscript.

Funding: This work was supported by a National Research Foundation of Korea (NRF) grant funded by the Korean government (MSIT; Ministry of Science and ICT) (No. 2020R1F1A1068242). This work was also supported by Nano-Material Technology Development Program through the NRF funded by the Ministry of Science, ICT and Future Planning (No. 2009-0082580). This work was partially supported by research fund of Chungnam National University.

Institutional Review Board Statement: Not applicable.

Informed Consent Statement: Not applicable.

Data Availability Statement: All data collected in this study are presented within this article and Supplementary Materials.

Conflicts of Interest: The authors declare no competing financial interest.

References

1. Bergveld, P. Development of an ion-sensitive solid-state device for neurophysiological measurements. *IEEE Trans. Biomed. Eng.* **1970**, *1*, 70–71. [CrossRef] [PubMed]
2. Zheng, G.; Patolsky, F.; Cui, Y.; Wang, W.U.; Lieber, C.M. Multiplexed electrical detection of cancer markers with nanowire sensor arrays. *Nat. Biotechnol.* **2005**, *23*, 1294–1301. [CrossRef]
3. Kim, A.; Ah, C.S.; Yu, H.Y.; Yang, J.-H.; Baek, I.-B.; Ahn, C.-G.; Park, C.W.; Jun, M.S.; Lee, S. Ultrasensitive, label-free, and real-time immunodetection using silicon field-effect transistors. *Appl. Phys. Lett.* **2007**, *91*, 103901. [CrossRef]
4. Tarasov, A.; Gray, D.W.; Tsai, M.-Y.; Shields, N.; Montrose, A.; Creedon, N.; Lovera, P.; O'Riordan, A.; Mooney, M.H.; Vogel, E.M. A potentiometric biosensor for rapid on-site disease diagnostics. *Biosens. Bioelectron.* **2016**, *79*, 669–678. [CrossRef]
5. Hahm, J.-i.; Lieber, C.M. Direct ultrasensitive electrical detection of DNA and DNA sequence variations using nanowire nanosensors. *Nano Lett.* **2004**, *4*, 51–54. [CrossRef]
6. Uslu, F.; Ingebrandt, S.; Mayer, D.; Böcker-Meffert, S.; Odenthal, M.; Offenhäusser, A. Labelfree fully electronic nucleic acid detection system based on a field-effect transistor device. *Biosens. Bioelectron.* **2004**, *19*, 1723–1731. [CrossRef]
7. Patolsky, F.; Zheng, G.; Hayden, O.; Lakadamyali, M.; Zhuang, X.; Lieber, C.M. Electrical detection of single viruses. *Proc. Natl. Acad. Sci. USA* **2004**, *101*, 14017–14022. [CrossRef] [PubMed]
8. Gu, B.; Park, T.J.; Ahn, J.H.; Huang, X.J.; Lee, S.Y.; Choi, Y.K. Nanogap field-effect transistor biosensors for electrical detection of avian influenza. *Small* **2009**, *5*, 2407–2412. [CrossRef] [PubMed]
9. Kwon, J.; Lee, Y.; Lee, T.; Ahn, J.-H. Aptamer-based field-effect transistor for detection of avian influenza virus in chicken serum. *Anal. Chem.* **2020**, *92*, 5524–5531. [CrossRef]
10. Cui, Y.; Wei, Q.; Park, H.; Lieber, C.M. Nanowire nanosensors for highly sensitive and selective detection of biological and chemical species. *Science* **2001**, *293*, 1289–1292. [CrossRef]
11. Stern, E.; Klemic, J.F.; Routenberg, D.A.; Wyrembak, P.N.; Turner-Evans, D.B.; Hamilton, A.D.; LaVan, D.A.; Fahmy, T.M.; Reed, M.A. Label-free immunodetection with CMOS-compatible semiconducting nanowires. *Nature* **2007**, *445*, 519–522. [CrossRef]
12. Ahn, J.-H.; Choi, S.-J.; Han, J.-W.; Park, T.J.; Lee, S.Y.; Choi, Y.-K. Double-gate nanowire field effect transistor for a biosensor. *Nano Lett.* **2010**, *10*, 2934–2938. [CrossRef]
13. Star, A.; Gabriel, J.-C.P.; Bradley, K.; Grüner, G. Electronic detection of specific protein binding using nanotube FET devices. *Nano Lett.* **2003**, *3*, 459–463. [CrossRef]
14. Cho, Y.; Pham Ba, V.A.; Jeong, J.-Y.; Choi, Y.; Hong, S. Ion-Selective Carbon Nanotube Field-Effect Transistors for Monitoring Drug Effects on Nicotinic Acetylcholine Receptor Activation in Live Cells. *Sensors* **2020**, *20*, 3680. [CrossRef] [PubMed]
15. Ang, P.K.; Chen, W.; Wee, A.T.S.; Loh, K.P. Solution-gated epitaxial graphene as pH sensor. *J. Am. Chem. Soc.* **2008**, *130*, 14392–14393. [CrossRef]
16. Ping, J.; Vishnubhotla, R.; Vrudhula, A.; Johnson, A.C. Scalable production of high-sensitivity, label-free DNA biosensors based on back-gated graphene field effect transistors. *ACS Nano* **2016**, *10*, 8700–8704. [CrossRef] [PubMed]
17. Ohno, Y.; Maehashi, K.; Yamashiro, Y.; Matsumoto, K. Electrolyte-gated graphene field-effect transistors for detecting pH and protein adsorption. *Nano Lett.* **2009**, *9*, 3318–3322. [CrossRef]
18. Sarkar, D.; Liu, W.; Xie, X.; Anselmo, A.C.; Mitragotri, S.; Banerjee, K. MoS_2 field-effect transistor for next-generation label-free biosensors. *ACS Nano* **2014**, *8*, 3992–4003. [CrossRef] [PubMed]
19. Chen, Y.; Ren, R.; Pu, H.; Chang, J.; Mao, S.; Chen, J. Field-effect transistor biosensors with two-dimensional black phosphorus nanosheets. *Biosens. Bioelectron.* **2017**, *89*, 505–510. [CrossRef] [PubMed]
20. Kim, J.; Rim, Y.S.; Chen, H.; Cao, H.H.; Nakatsuka, N.; Hinton, H.L.; Zhao, C.; Andrews, A.M.; Yang, Y.; Weiss, P.S. Fabrication of high-performance ultrathin In_2O_3 film field-effect transistors and biosensors using chemical lift-off lithography. *Acs Nano* **2015**, *9*, 4572–4582. [CrossRef] [PubMed]
21. Li, C.; Curreli, M.; Lin, H.; Lei, B.; Ishikawa, F.; Datar, R.; Cote, R.J.; Thompson, M.E.; Zhou, C. Complementary detection of prostate-specific antigen using In_2O_3 nanowires and carbon nanotubes. *J. Am. Chem. Soc.* **2005**, *127*, 12484–12485. [CrossRef]
22. Liu, Q.; Aroonyadet, N.; Song, Y.; Wang, X.; Cao, X.; Liu, Y.; Cong, S.; Wu, F.; Thompson, M.E.; Zhou, C. Highly sensitive and quick detection of acute myocardial infarction biomarkers using In_2O_3 nanoribbon biosensors fabricated using shadow masks. *ACS Nano* **2016**, *10*, 10117–10125. [CrossRef] [PubMed]
23. Nair, P.R.; Alam, M.A. Design considerations of silicon nanowire biosensors. *IEEE Trans. Electron Devices* **2007**, *54*, 3400–3408. [CrossRef]
24. Kaisti, M. Detection principles of biological and chemical FET sensors. *Biosens. Bioelectron.* **2017**, *98*, 437–448. [CrossRef]
25. Ahn, J.-H.; Choi, B.; Choi, S.-J. Understanding the signal amplification in dual-gate FET-based biosensors. *J. Appl. Phys.* **2020**, *128*, 184502. [CrossRef]

26. Chen, S.; Bomer, J.G.; Carlen, E.T.; van den Berg, A. Al_2O_3/silicon nanoISFET with near ideal Nernstian response. *Nano Lett.* **2011**, *11*, 2334–2341. [CrossRef] [PubMed]
27. Tarasov, A.; Wipf, M.; Bedner, K.; Kurz, J.; Fu, W.; Guzenko, V.A.; Knopfmacher, O.; Stoop, R.L.; Calame, M.; Schönenberger, C. True Reference Nanosensor Realized with Silicon Nanowires. *Langmuir* **2012**, *28*, 9899–9905. [CrossRef]
28. So, H.-M.; Won, K.; Kim, Y.H.; Kim, B.-K.; Ryu, B.H.; Na, P.S.; Kim, H.; Lee, J.-O. Single-walled carbon nanotube biosensors using aptamers as molecular recognition elements. *J. Am. Chem. Soc.* **2005**, *127*, 11906–11907. [CrossRef] [PubMed]
29. Goda, T.; Miyahara, Y. A hairpin DNA aptamer coupled with groove binders as a smart switch for a field-effect transistor biosensor. *Biosens. Bioelectron.* **2012**, *32*, 244–249. [CrossRef]
30. Nakatsuka, N.; Yang, K.-A.; Abendroth, J.M.; Cheung, K.M.; Xu, X.; Yang, H.; Zhao, C.; Zhu, B.; Rim, Y.S.; Yang, Y. Aptamer–field-effect transistors overcome Debye length limitations for small-molecule sensing. *Science* **2018**, *362*, 319–324. [CrossRef]
31. Han, S.H.; Kim, S.K.; Park, K.; Yi, S.Y.; Park, H.-J.; Lyu, H.-K.; Kim, M.; Chung, B.H. Detection of mutant p53 using field-effect transistor biosensor. *Ana. Chim. Acta* **2010**, *665*, 79–83. [CrossRef]
32. Huang, Y.-W.; Wu, C.-S.; Chuang, C.-K.; Pang, S.-T.; Pan, T.-M.; Yang, Y.-S.; Ko, F.-H. Real-Time and Label-Free Detection of the Prostate-Specific Antigen in Human Serum by a Polycrystalline Silicon Nanowire Field-Effect Transistor Biosensor. *Anal. Chem.* **2013**, *85*, 7912–7918. [CrossRef]
33. Cai, B.; Huang, L.; Zhang, H.; Sun, Z.; Zhang, Z.; Zhang, G.-J. Gold nanoparticles-decorated graphene field-effect transistor biosensor for femtomolar MicroRNA detection. *Biosens. Bioelectron.* **2015**, *74*, 329–334. [CrossRef] [PubMed]
34. Rothberg, J.M.; Hinz, W.; Rearick, T.M.; Schultz, J.; Mileski, W.; Davey, M.; Leamon, J.H.; Johnson, K.; Milgrew, M.J.; Edwards, M. An integrated semiconductor device enabling non-optical genome sequencing. *Nature* **2011**, *475*, 348–352. [CrossRef]
35. Li, H.; Liu, X.; Li, L.; Mu, X.; Genov, R.; Mason, A.J. CMOS electrochemical instrumentation for biosensor microsystems: A review. *Sensors* **2017**, *17*, 74. [CrossRef] [PubMed]
36. Kim, Y.; Chortos, A.; Xu, W.; Liu, Y.; Oh, J.Y.; Son, D.; Kang, J.; Foudeh, A.M.; Zhu, C.; Lee, Y. A bioinspired flexible organic artificial afferent nerve. *Science* **2018**, *360*, 998–1003. [CrossRef]
37. Wan, C.; Chen, G.; Fu, Y.; Wang, M.; Matsuhisa, N.; Pan, S.; Pan, L.; Yang, H.; Wan, Q.; Zhu, L. An artificial sensory neuron with tactile perceptual learning. *Adv. Mater.* **2018**, *30*, 1801291. [CrossRef] [PubMed]
38. Seo, S.; Jo, S.-H.; Kim, S.; Shim, J.; Oh, S.; Kim, J.-H.; Heo, K.; Choi, J.-W.; Choi, C.; Oh, S. Artificial optic-neural synapse for colored and color-mixed pattern recognition. *Nat. Commun.* **2018**, *9*, 5106. [CrossRef]
39. Yoon, J.H.; Wang, Z.; Kim, K.M.; Wu, H.; Ravichandran, V.; Xia, Q.; Hwang, C.S.; Yang, J.J. An artificial nociceptor based on a diffusive memristor. *Nat. Commun.* **2018**, *9*, 417. [CrossRef]
40. Han, J.-K.; Geum, D.-M.; Lee, M.-W.; Yu, J.-M.; Kim, S.K.; Kim, S.; Choi, Y.-K. Bioinspired Photoresponsive Single Transistor Neuron for a Neuromorphic Visual System. *Nano Lett.* **2020**, *20*, 8781–8788. [CrossRef]
41. Bartolozzi, C.; Indiveri, G. Synaptic dynamics in analog VLSI. *Neural Comput.* **2007**, *19*, 2581–2603. [CrossRef]
42. Maass, W. Networks of spiking neurons: The third generation of neural network models. *Neural Netw.* **1997**, *10*, 1659–1671. [CrossRef]
43. Kwon, J.; Lee, B.-H.; Kim, S.-Y.; Park, J.-Y.; Bae, H.; Choi, Y.-K.; Ahn, J.-H. Nanoscale FET-based transduction toward sensitive extended-gate biosensors. *ACS Sens.* **2019**, *4*, 1724–1729. [CrossRef] [PubMed]
44. Pullano, S.A.; Critello, C.D.; Mahbub, I.; Tasneem, N.T.; Shamsir, S.; Islam, S.K.; Greco, M.; Fiorillo, A.S. EGFET-based sensors for bioanalytical applications: A review. *Sensors* **2018**, *18*, 4042. [CrossRef]
45. Tarasov, A.; Wipf, M.; Stoop, R.L.; Bedner, K.; Fu, W.; Guzenko, V.A.; Knopfmacher, O.; Calame, M.; Schönenberger, C. Understanding the electrolyte background for biochemical sensing with ion-sensitive field-effect transistors. *ACS Nano* **2012**, *6*, 9291–9298. [CrossRef] [PubMed]
46. Kwon, J.; Yoo, Y.K.; Lee, J.H.; Ahn, J.-H. pH Sensing Characteristics of Extended-Gate Field-Effect Transistor with Al_2O_3 Layer. *J. Nanosci. Nanotechnol.* **2019**, *19*, 6682–6686. [CrossRef]
47. Gutiérrez-Sanz, Ó.; Andoy, N.M.; Filipiak, M.S.; Haustein, N.; Tarasov, A. Direct, Label-Free, and Rapid Transistor-Based Immunodetection in Whole Serum. *ACS Sens.* **2017**, *2*, 1278–1286. [CrossRef] [PubMed]
48. Gao, N.; Gao, T.; Yang, X.; Dai, X.; Zhou, W.; Zhang, A.; Lieber, C.M. Specific detection of biomolecules in physiological solutions using graphene transistor biosensors. *Proc. Natl. Acad. Sci. USA* **2016**, *113*, 14633. [CrossRef] [PubMed]
49. Spijkman, M.J.; Brondijk, J.J.; Geuns, T.C.; Smits, E.C.; Cramer, T.; Zerbetto, F.; Stoliar, P.; Biscarini, F.; Blom, P.W.; de Leeuw, D.M. Dual-gate organic field-effect transistors as potentiometric sensors in aqueous solution. *Adv. Func. Mater.* **2010**, *20*, 898–905. [CrossRef]
50. Knopfmacher, O.; Tarasov, A.; Fu, W.; Wipf, M.; Niesen, B.; Calame, M.; Schonenberger, C. Nernst limit in dual-gated Si-nanowire FET sensors. *Nano Lett.* **2010**, *10*, 2268–2274. [CrossRef]
51. Weste, N.H.; Harris, D. *CMOS VLSI design: A circuits and systems perspective*, 4th ed.; Pearson Education India: Chennai, India, 2010.
52. Liu, Q.; Liu, Y.; Wu, F.; Cao, X.; Li, Z.; Alharbi, M.; Abbas, A.N.; Amer, M.R.; Zhou, C. Highly sensitive and wearable In_2O_3 nanoribbon transistor biosensors with integrated on-chip gate for glucose monitoring in body fluids. *ACS Nano* **2018**, *12*, 1170–1178. [CrossRef] [PubMed]
53. Choi, D.-H.; Li, Y.; Cutting, G.R.; Searson, P.C. A wearable potentiometric sensor with integrated salt bridge for sweat chloride measurement. *Sens. Actuators B* **2017**, *250*, 673–678. [CrossRef]

54. Go, J.; Nair, P.R.; Reddy Jr, B.; Dorvel, B.; Bashir, R.; Alam, M.A. Coupled heterogeneous nanowire–nanoplate planar transistor sensors for giant (> 10 V/pH) Nernst response. *ACS Nano* **2012**, *6*, 5972–5979. [CrossRef] [PubMed]
55. Zhang, D.; Lu, Y.; Zhang, Q.; Liu, L.; Li, S.; Yao, Y.; Jiang, J.; Liu, G.L.; Liu, Q. Protein detecting with smartphone-controlled electrochemical impedance spectroscopy for point-of-care applications. *Sens. Actuators B* **2016**, *222*, 994–1002. [CrossRef]
56. Sahatiya, P.; Kadu, A.; Gupta, H.; Thanga Gomathi, P.; Badhulika, S. Flexible, Disposable Cellulose-Paper-Based MoS_2/Cu_2S Hybrid for Wireless Environmental Monitoring and Multifunctional Sensing of Chemical Stimuli. *ACS Appl. Mater. Interfaces* **2018**, *10*, 9048–9059. [CrossRef] [PubMed]